Modeling of the Biotransformation Processes

A. Vrsalović Presečki, Z. Findrik, and B. Zelić*
Faculty of Chemical Engineering and Technology, University of Zagreb,
Marulićev trg 19, HR-10000 Zagreb, Croatia
e-Mail: bzelic@fkit.hr, Phone: +385 (0) 1 4597 146,
Fax: +385 (0) 1 4597 133

Original scientific paper
Received: April 5, 2006
Accepted: May 26, 2006

Dedicated to Prof. Dr. Đurđa Vasić-Rački on occasion of her 60th birthday

Modeling and simulation of biotransformation processes have a large potential in searching for optimal process conditions, development and process design, control, scale-up, identifying of the process cost structure, and comparing process alternatives. Modeling and simulation leads to better understanding and quantification of the investigated process and could lead to significant material and costs savings especially in the early phases of the process development. In this review modeling and simulation techniques are demonstrated on two basically different types of bioprocesses, enzymatic and microbial biotransformations. Acetophenone reduction catalyzed by ADH from *Thermoanaerobacter* sp., amino acid oxidation catalyzed by D-amino acid oxidase from *Arthrobacter protophormiae,* and L-DOPA oxidation catalyzed by L-amino acid oxidases from *Crotalus adamanteus* and *Rhodococcus opacus* are examples for modeling of enzymatic biotransformation processes. On the other hand, microbial biotransformation processes are shown for: production of alcohol dehydrogenase (ADH) in baker's yeast growing cells, production of L-malic acid by permeabilized non-growing yeast cells, production of 2,5-diketo-D-gluconic acid using *Pantoea citrea*, and for *Escherichia coli* based pyruvate production.

Key words:
Modeling, enzymatic biotransformation, microbial biotransformation

Introduction

Biotransformations are chemically well defined enzyme catalyzed reactions in which pure substances-reactants are being transformed in structural more or less similar products. These reactions are catalyzed by either pure enzymes (enzymatic biotransformations) or by enzymes in whole cells of microorganisms (microbial biotransformations). The essential difference between microbial biotransformation and enzymatic biotransformation is in the number of reaction steps. There are several catalytic steps between the substrate and the product in microbial biotransformation, while there are only one or two steps in the enzymatic biotransformation, respectively. The distinction is also in the fact that the chemical structure of the substrate and the product resemble one another in the enzymatic biotransformation, but not necessarily in the microbial biotransformation. Furthermore, microbial biotransformation should concern all specific properties and demands of microbial biomass.[1]

In bio-industries, there is a strong demand for systems which are optimized and automatically controlled biological processes because of their complexity resulting in labor-intensive operation. Additionally, early phases of process development are crucial for determining production costs incurred and environmental burdens caused when production begins. Due to the competitive conditions between companies, new processes have to be optimized early during their development considering all relevant boundary conditions concerning technical feasibility, economy, environment, safety, and health. Modeling and simulation of the process in these phases can provide a sound basis for an economic and ecological evaluations that enables an integrated optimization of the process. A first ecological assessment can be based on the material and energy balance of the process to identify the most relevant materials and process steps. Additionally, process simulation results can also be used for a more detailed environmental assessment.[2]

Information gathered from the model simulations are intended for decision making, to draw conclusions for automatic control actions of biological states, or to initiate specific activities in experimentation, production or regulatory work. Model necessary for a given process is usually not directly available, and its development is a laborious and expensive stage in the whole process development and optimization procedure. Reliable models

*Corresponding author
Contract grant sponsor: Croatian Ministry of Science, Education, and Sport
Contract grant number: 0125 021

should have good interpolation and extrapolation properties in order to predict system behavior within and outside the range of experimental data.[3] It is highly desirable for models to be as simple as possible, but not too simple. Still they have to describe the process faithfully, include a procedure which accounts for external uncertainties or unforeseen changes in a process, and provide relatively simple implementation aspects.

Modeling of biotransformation processes is based on the knowledge of mass balances, transport phenomena, and reaction kinetics obtained by profound microbiological/biochemical studies. After the selection of an appropriate model structure, one encounters the issue of finding a unique set of corresponding model parameters (which have to be estimated from experimental data). If the theoretical identifiability of the parameters can be proved, very often the associated confidence space which is calculated during the experimental data fitting is quite large (problem of uniqueness). A unique identification of the model parameters is only possible if the available data are sufficiently rich.[4]

In mathematical modeling of biotransformation processes, equations are formulated involving Michaelis-Menten's or Monod's kinetics, which are often modified reflecting product and/or substrate inhibition. In addition, equations can also be written based upon carbon and nitrogen balances and in some cases, compounds containing high energy phosphate bonds.

Existing modeling strategies can be divided into white box, black box, and gray box. In the white box modeling strategy, the model development is mainly driven by the knowledge of the relevant biochemical and physical mechanisms. The resulting models are intended to be generally applicable, but at the same time they require an extensive research program to reveal all relevant mechanisms and to quantify these mechanisms correctly. In a black box modeling strategy, the model development is mainly driven by measured data from the actual system that has to be modeled. The main advantage of the use of the black box modeling strategies is the fact that, within reasonable amount of time, one can obtain a highly accurate mathematical model within experimental data without detailed knowledge of a system. A gray box modeling strategy can be defined as a suitable combination of a black box and white box strategy, which leads to models with a short development time, and good interpolation and extrapolation properties.[3]

Models that describe a process faithfully are often very complex, and, when used in conjunction with the optimization procedure, computation problems may arise. If, alternatively, simple models with time-varying parameters are used, it is possible that suboptimal results will be obtained. As many biochemical processes involve a large number of species or unknown reaction mechanisms, construction of reliable analytical model is time-consuming and not cost effective.[5] Almost all of the modeling studies, reported in the literature, are either theoretical or based on the laboratory scale data, while those that have an experimental comparison with industrial data are very limited. Therefore, the available models have either a limited range of applicability or represent behavioral inconsistencies with industrial data.[6] However, such a model based approach has rarely succeeded in the optimization and control of the actual operations of microbial production plants due to the difficulty in developing mathematical model capable to describe the complex intracellular reactions of the microorganisms involved. Therefore, the operational conditions of industrial fermentation processes are often optimized through knowledge-based operations under the control of highly skilled operators. While such empirical knowledge-based operations can be considered as a useful and practical, it is difficult to adapt them to computer control by traditional methods. Namely, the involved skills cannot often be quantified or incorporated into a traditional control system. To overcome this shortcoming, a knowledge based approach including fuzzy control, artificial neural network, expert system, genetic algorithm etc. have been introduced in the biotechnology field over the last two decades.[7]

Usually, mathematical models for the microbial biotransformation processes are divided in two mayor groups, unstructured and structured mathematical models. Unstructured mathematical models of the microbiological systems, which assume the biomass population as a structureless, featureless entity have been utilized for the representation of the culture dynamics in the exponential and stationary phases of growth. In general, unstructured models are based on Monod's rate equations, where growth depends on biomass concentration as well as on a sole limiting substrate. The unstructured model allows determination of the respective proportion of substrates used for biosynthesis and cell maintenance, and also the respective proportion of metabolite productions associated with biosynthesis and cell maintenance.[8] However, they are unable to describe long lag phase in batch culture and transient responses during unsteady conditions. Structured model can describe transient growth and characterize microbial population under a wide variety of dynamic growth conditions. Ideally, an appropriate mathematical model should consider concentrations of all the chemical substances in the culture environment, and inside the microorganism, for proper elucidation of biochemical reaction mechanisms involved in the culture metabolism.[9]

The modeling of the enzyme reaction kinetics as a tool for enzyme reaction engineering plays an important role in developing the enzyme-catalyzed reaction for large-scale production. Modeling of the

enzyme kinetics and the reactors can be used to find optimal operation points and to increase our knowledge about the process[10] and facilitate identification of the most effective reactor mode of operation.[11] For design of an enzyme reactor a detailed knowledge of the kinetic parameters of the catalyst under operational conditions is essential.[12]

This paper is an attempt to describe the current state in the modeling of the biotransformation processes. The aim is not to present a review of the literature, but to briefly report about similarities and differences between modeling and simulation of enzymatic and microbial biotransformation processes. Therefore, a significant amount of the models, estimated parameters and simulation results are included and used to illustrate when and how modeling of the biotransformation processes can be used and to demonstrate its limitations. For detailed information on the experimental data, experimental and theoretical procedures, and theoretical analyses and their application of the biotransformation processes presented in this report, the reader is referred to recent publications by our group.[14,16,17,23,29,33–36]

Mathematical models of enzymatic biotransformation processes

Acetophenone reduction catalyzed by ADH from *Thermoanaerobacter* sp.

Chiral alcohols are important building blocks for the synthesis of pharmaceuticals, pesticides, pheromones, flavours, fragrances and advanced materials such as liquid crystals.[13] Stereoselective reduction of ketones is the basic way to produce them. In this example (*S*)-1-phenylethanol is synthesized from acetophenone by the action of alcohol dehydrogenase from *Thermoanaerobacter* sp. (ADH). The enzyme is interesting because of its thermophilic origin which makes it active and stable at higher temperatures than it is usual for enzymes.[14]

It is known that dehydrogenases require the presence of coenzyme for their activity (in the stoichiometric amounts to the substrate). If the coenzyme is regenerated by the known methods,[15] it can be added in lower concentration. In addition, the reaction equilibrium is shifted to the side of alcohol production by removing the oxidized form of coenzyme ($NADP^+$) from the reaction system. In the reaction of acetophenone reduction two cases are considered: acetophenone reduction without (Fig. 1A) and with coenzyme regeneration (Fig. 1B). Substrate coupled system is used for the coenzyme regeneration and 2-propanol as a regenerating substrate added in the system. For both systems detailed enzyme kinetics were determined by the initial reaction rate method. In such complex system many interactions between reaction components occur, which can be seen from the number of estimated parameters (Table 1).

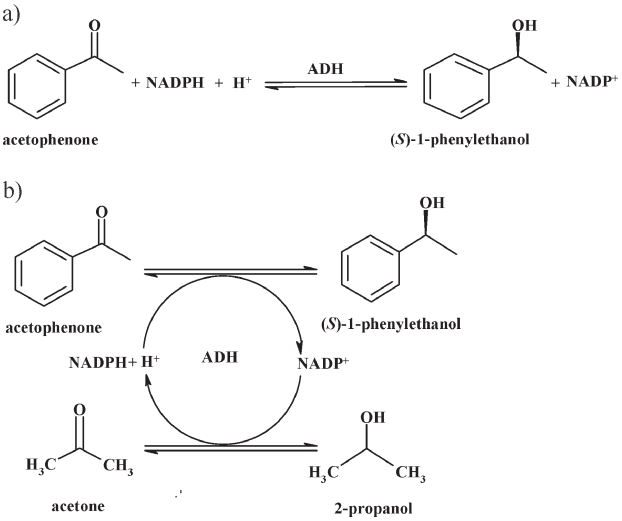

Fig. 1 – *Acetophenone reduction: a) without and b) with* NADPH *regeneration*

Table 1 – *Kinetic parameters for acetophenone reduction catalyzed by alcohol dehydrogenase from Thermoanaerobacter* sp.

Parameter	Unit	Value
$K_m^{\text{acetophenone}}$	mmol dm^{-3}	0.034
$K_m^{(S)\text{-1-phenylethanol}}$	mmol dm^{-3}	0.112
K_m^{acetone}	mmol dm^{-3}	1.091
$K_m^{\text{2-propanol}}$	mmol dm^{-3}	0.408
K_m^{NADPH}	mmol dm^{-3}	0.004
$K_m^{\text{NADP}^+}$	mmol dm^{-3}	0.007
$K_{i1}^{(S)\text{-1-phenylethanol}}$	mmol dm^{-3}	0.070
K_{i1}^{acetone}	mmol dm^{-3}	0.899
$K_{i1}^{\text{2-propanol}}$	mmol dm^{-3}	10.973
$K_{i1}^{\text{NADP}^+}$	mmol dm^{-3}	0.017
$K_{i1}^{\text{acetophenone}}$	mmol dm^{-3}	6.077
$K_{i2}^{\text{acetophenone}}$	mmol dm^{-3}	0.010
K_{i2}^{acetone}	mmol dm^{-3}	7.576
$K_{i2}^{\text{2-propanol}}$	mmol dm^{-3}	0.079
K_{i2}^{NADPH}	mmol dm^{-3}	0.006
$K_{i3}^{\text{2-propanol}}$	mmol dm^{-3}	20.303
$K_{i3}^{(S)\text{-1-phenylethanol}}$	mmol dm^{-3}	0.535
$K_{i3}^{\text{acetophenone}}$	mmol dm^{-3}	1.886
$K_{i3}^{\text{NADP}^+}$	mmol dm^{-3}	0.005
K_{i4}^{acetone}	mmol dm^{-3}	2.242
$K_{i4}^{\text{acetophenone}}$	mmol dm^{-3}	0.348
$K_{i4}^{(S)\text{-1-phenylethanol}}$	mmol dm^{-3}	29.551
K_{i4}^{NADPH}	mmol dm^{-3}	0.007
$K_{i4}^{\text{2-propanol}}$	mmol dm^{-3}	288.016

Based on the estimated parameters, mathematical model was developed for a batch and a continuous stirred tank reactor (Fig. 2). It was demonstrated by the batch reactor experiments that the reaction equilibrium of acetophenone reduction without coenzyme regeneration is shifted to the side of the acetophenone (Fig. 3A). The developed model for acetophenone reduction without coenzyme regeneration was experimentally validated. Reaction kinetics has been described as a double-substrate Michaelis-Menten equation taking into consideration presence of substrate (acetophenone) inhibition, and competitive inhibition of both reaction products – (*S*)-1-phenylethanol and $NADP^+$. These inhibitions were quantified by the corresponding inhibition constants (Table 1).

Acetophenone reduction with coenzyme regeneration was carried out in the batch, repetitive batch and continuous stirred tank reactor. Batch experiment (Fig. 3A) validated the developed mathematical model, and proved that coenzyme regeneration shifts the reaction equilibrium to the side of (*S*)-1-phenylethanol**.** Repetitive batch experiment (Fig. 3B) showed that enzyme loses its activity in the second batch, which is supported by the estimated V_m parameters (Table 2). Mathematical model made it possible to find the optimal initial concentration of $NADP^+$ and 2-propanol for repetitive batch experiment as well as for the CSTR experiment. CSTR experiment (Fig. 3C) carried out in the enzyme membrane reactor revealed significant enzyme deactivation which was described by the first order deactivation kinetics. Besides for determination of the optimal initial conditions, in the reactor experiments by mathematical modeling made it possible to find the best reactor mode for the synthesis of (*S*)-1-phenylethanol at the lowest coenzyme cost.

$$r_1 = \frac{V_{m1}\cdot \mathrm{e}^{-k_d\cdot t}\cdot c_{\text{acetophenone}}}{\left(c_{\text{acetophenone}} + K_m^{\text{acetophenone}}\cdot\left(1+\frac{c_{(S)\text{-1-phenylethanol}}}{K_{i1}^{\text{phenylethanol}}}+\frac{c_{\text{acetone}}}{K_{i1}^{\text{acetone}}}+\frac{c_{\text{2-propanol}}}{K_{i1}^{\text{2-propanol}}}\right)+\frac{c_{\text{acetophenone}}^2}{K_{i1}^{\text{acetophenone}}}\right)}\cdot\frac{c_{\text{NADPH}}}{\left(c_{\text{NADPH}}+K_m^{\text{NADPH}}\cdot\left(1+\frac{c_{\text{NADP}^+}}{K_{i1}^{\text{NADP}^+}}\right)\right)}$$

$$r_2 = \frac{V_{m2}\cdot \mathrm{e}^{-k_d\cdot t}\cdot c_{(S)\text{-1-phenylethanol}}}{\left(c_{(S)\text{-1-phenylethanol}} + K_m^{(S)\text{-1-phenylethanol}}\cdot\left(1+\frac{c_{\text{acetophenone}}}{K_{i2}^{\text{acetophenone}}}+\frac{c_{\text{acetone}}}{K_{i2}^{\text{acetone}}}+\frac{c_{\text{2-propanol}}}{K_{i2}^{\text{2-propanol}}}\right)\right)}\cdot\frac{c_{\text{NADP}^+}}{\left(c_{\text{NADP}^+}+K_m^{\text{NADP}^+}\cdot\left(1+\frac{c_{\text{NADPH}}}{K_{i2}^{\text{NADPH}}}\right)\right)}$$

$$r_3 = \frac{V_{m3}\cdot \mathrm{e}^{-k_d\cdot t}\cdot c_{\text{acetone}}}{\left(c_{\text{acetone}} + K_m^{\text{acetone}}\cdot\left(1+\frac{c_{(S)\text{-1-phenylethanol}}}{K_{i3}^{(S)\text{-1-phenylethanol}}}+\frac{c_{\text{acetophenone}}}{K_{i3}^{\text{acetophenone}}}+\frac{c_{\text{2-propanol}}}{K_{i3}^{\text{2-propanol}}}\right)\right)}\cdot\frac{c_{\text{NADPH}}}{\left(c_{\text{NADPH}}+K_m^{\text{NADPH}}\cdot\left(1+\frac{c_{\text{NADP}^+}}{K_{i3}^{\text{NADP}^+}}\right)\right)}$$

$$r_4 = \frac{V_{m4}\cdot \mathrm{e}^{-k_d\cdot t}\cdot c_{\text{2-propanol}}}{\left(c_{\text{2-propanol}} + K_m^{\text{2-propanol}}\cdot\left(1+\frac{c_{(S)\text{-1-phenylethanol}}}{K_{i4}^{(S)\text{-1-phenylethanol}}}+\frac{c_{\text{acetone}}}{K_{i4}^{\text{acetone}}}+\frac{c_{\text{acetophenone}}}{K_{i4}^{\text{acetophenone}}}\right)+\frac{c_{\text{2-propanol}}^2}{\mathrm{K}_{\mathrm{i4}}^{\text{2-propanol}}}\right)}\cdot\frac{c_{\text{NADP}^+}}{\left(c_{\text{NADP}^+}+K_m^{\text{NADP}^+}\cdot\left(1+\frac{c_{\text{NADPH}}}{K_{i4}^{\text{NADPH}}}\right)\right)}$$

• Without coenzyme regeneration: c_{acetone}, $c_{\text{2-propanol}} = 0$; r_3, $r_4 = 0$; If no enzyme deactivation occurs, $k_d = 0$.

Mass balance equations in the batch reactor

$$\frac{\mathrm{d}c_{\text{acetophenone}}}{\mathrm{d}t} = -r_1 + r_2$$

$$\frac{\mathrm{d}c_{(S)\text{-1-phenylethanol}}}{\mathrm{d}t} = r_1 - r_2$$

$$\frac{\mathrm{d}c_{\text{acetone}}}{\mathrm{d}t} = -r_3 + r_4$$

$$\frac{\mathrm{d}c_{\text{2-propanol}}}{\mathrm{d}t} = r_3 - r_4$$

$$\frac{\mathrm{d}c_{\text{NADPH}}}{\mathrm{d}t} = -r_1 + r_2 - r_3 + r_4$$

$$\frac{\mathrm{d}c_{\text{NADP}^+}}{\mathrm{d}t} = r_1 - r_2 + r_3 - r_4$$

Mass balance equations in CSTR

$$\frac{\mathrm{d}c_{\text{acetophenone}}}{\mathrm{d}t} = \frac{c_{\text{acetophenone0}} - c_{\text{acetophenone}}}{\tau} - r_1 + r_2$$

$$\frac{\mathrm{d}c_{(S)\text{-1-phenylethanol}}}{\mathrm{d}t} = \frac{c_{(S)\text{-1-phenylethanol0}} - c_{(S)\text{-1-phenylethanol}}}{\tau} + r_1 - r_2$$

$$\frac{\mathrm{d}c_{\text{acetone}}}{\mathrm{d}t} = \frac{c_{\text{acetone0}} - c_{\text{acetone}}}{\tau} - r_3 + r_4$$

$$\frac{\mathrm{d}c_{\text{2-propanol}}}{\mathrm{d}t} = \frac{c_{\text{2-propanol0}} - c_{\text{2-propanol}}}{\tau} + r_3 - r_4$$

$$\frac{\mathrm{d}c_{\text{NADPH}}}{\mathrm{d}t} = \frac{c_{\text{NADPH0}} - c_{\text{NADPH}}}{\tau} - r_1 + r_2 - r_3 + r_4$$

$$\frac{\mathrm{d}c_{\text{NADP}^+}}{\mathrm{d}t} = \frac{c_{\text{NADP}^+0} - c_{\text{NADP}^+}}{\tau} + r_1 - r_2 + r_3 - r_4$$

Fig. 2 – *Mathematical models for the acetophenone reduction in various types of reactors*

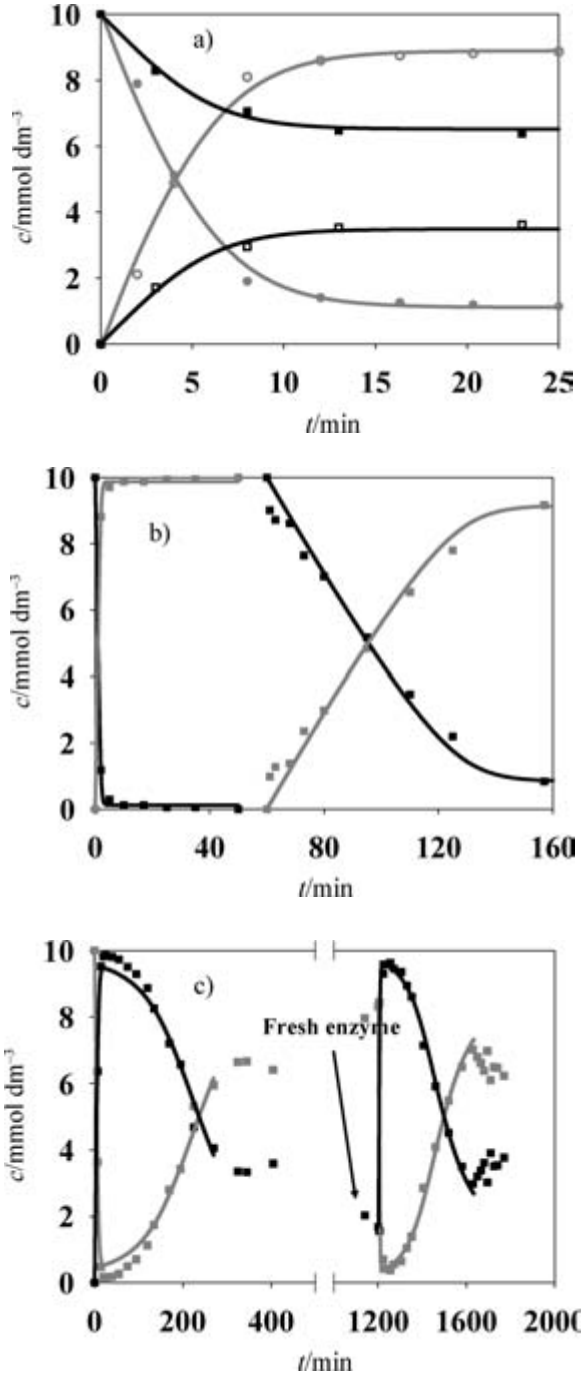

Fig. 3 – *a) Acetophenone reduction in the batch experiment. Without (● acetophenone and ○ (S)-1-phenylethanol concentration, — model) and with NADPH regeneration (■ acetophenone and □ (S)-1-phenylethanol concentration, — model). b) Acetophenone reduction with NADPH regeneration in the repetitive batch experiment (■ acetophenone and □ (S)-1-phenylethanol concentration). c) Acetophenone reduction with coenzyme regeneration in the continuous stirred tank reactor (enzyme membrane reactor) (□ acetophenone and ■ (S)-1-phenylethanol concentration).*

Table 2 – *Estimated maximal reaction rates for acetophenone reduction in different reactor experiments*

Parameter	Value	
Batch reactor without coenzyme regeneration		
V_{m1}, U cm^{-3}	1.47	
V_{m2}, U cm^{-3}	42.96	
Batch reactor with coenzyme regeneration		
V_{m1}, U cm^{-3}	5.85	
V_{m2}, U cm^{-3}	201.77	
V_{m3}, U cm^{-3}	4.41	
V_{m4}, U cm^{-3}	5.88	
Continuous stirred tank reactor with cofactor regeneration		
V_{m1}, U cm^{-3}	10.23	
V_{m2}, U cm^{-3}	205.69	
V_{m3}, U cm^{-3}	5.31	
V_{m4}, U cm^{-3}	8.25	
k_d, min^{-1}	0.014	
Repetitive batch with cofactor regeneration		
	1st cycle	2nd cycle
V_{m1}, U cm^{-3}	40.78	9.16
V_{m2}, U cm^{-3}	704.32	175.01
V_{m3}, U cm^{-3}	14.71	3.26
V_{m4}, U cm^{-3}	38.75	0.97

Amino acid oxidation catalyzed by D-amino acid oxidase from *Arthrobacter protophormiae*

One of the ways to prepare optically pure amino acid from their racemate is by action of stereospecific amino acid oxidases. If L-amino acid is to be prepared, than the activity of D-amino acid oxidase is required. In this example of enzyme kinetic modeling D-amino acid is being oxidized by D-amino acid from *Arthrobacter protophormiae.*[16] The reaction scheme is presented in Fig. 4. D-methionine is oxidized to 2-oxo-4-methylthiobutyric acid. Hydrogen peroxide that originates in this reaction is being removed from the system by adding the excess catalase. If catalase is not added, hydrogen peroxide reacts with α-keto acid in the reaction of oxidative decarboxylation forming the corresponding carboxylic acid (3-methylthiopropanoic acid).

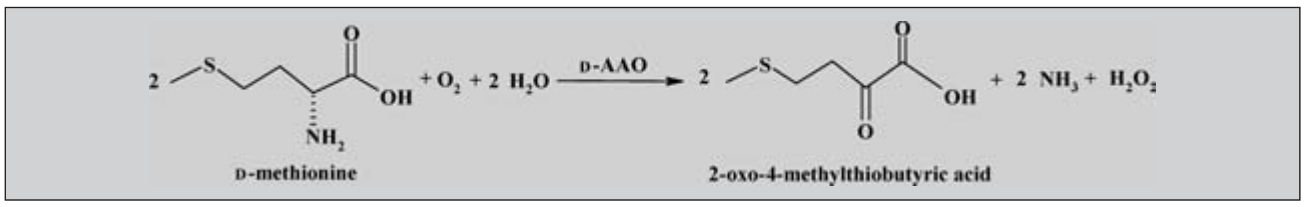

Fig. 4 – *D-methionine oxidation to 2-oxo-4-methylthiobutyric acid catalyzed by D-amino acid oxidase*

Enzyme kinetics of this reaction was described by Michaelis-Menten equation with competitive product inhibition. Kinetic parameters (Table 3) were estimated by non-linear regression from the independent experiments. Mathematical model (Fig. 5) was validated in the batch reactor experiments carried out with (Fig. 6a) and without (Fig. 6b) the presence of catalase.

$$r = \frac{V_m \cdot c_{\text{D-methionine}}}{K_m^{\text{D-methionine}} \cdot \left(1 + \frac{c_{\text{2-oxo-4-methylthiobutyric acid}}}{K_i^{\text{2-oxo-4-methylthiobutyric acid}}}\right) + c_{\text{D-methionine}}}$$

$$V_m = V_{m0} \cdot \mathrm{e}^{-k_d \cdot t}$$

$$\frac{\mathrm{d}c_{\text{D-methionine}}}{\mathrm{d}t} = -r$$

$$\frac{\mathrm{d}c_{\text{2-oxo-4-methylthiobutyric acid}}}{\mathrm{d}t} = r$$

Fig. 5 – *Mathematical model of D-methionine oxidation by D-amino acid oxidase from Arthrobacter protophormiae in the batch reactor*

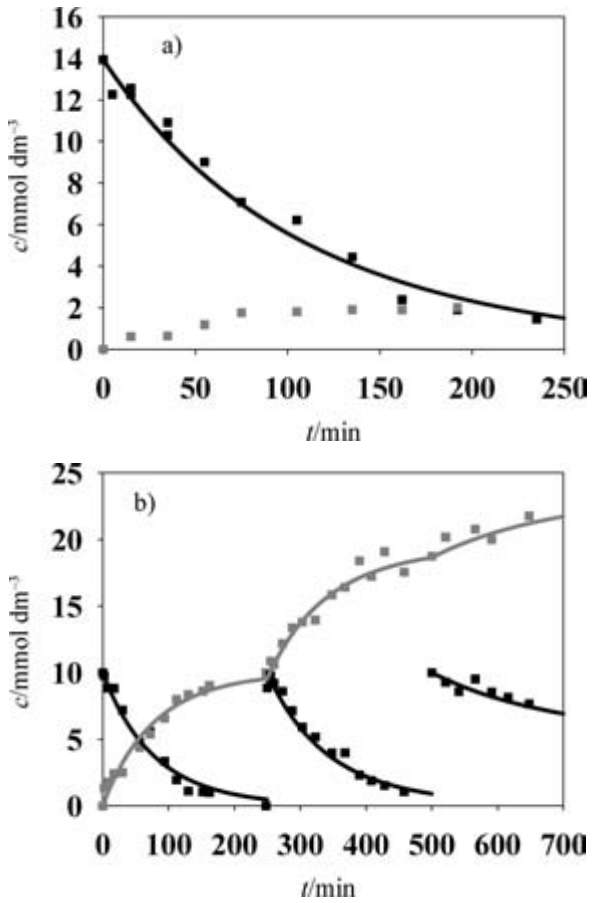

Fig. 6 – *D-methionine oxidation catalyzed by D-AAO from Arthrobacter protophormiae in the batch reactor A) without addition of catalase and B) with addition of catalase.* ■ *D-methionine and* ■ *2-oxo-4-methylthiobutyric acid, line – model simulation)*

Table 3 – *Kinetic parameters for D-methionine oxidation catalyzed by D-amino acid oxidase from Arthrobacter protophormiae*

Parameter	Unit	Value
$V_m^{\text{D-Met}}$	U cm^{-3}	20.01
$V_m^{\text{D-met}}$	mmol dm^{-3}	0.24
$V_m^{\text{2-oxo-4-methylthiobutyric acid}}$	mmol dm^{-3}	0.22
k_d (2nd batch)	min^{-1}	0.0007
k_d (3rd batch)	min^{-1}	0.0033

Since the proposed mathematical model could simulate the data well it was possible to conclude that secondary products that include hydrogen peroxide and 3-methylthiopropanoic acid do not inhibit the enzyme. In the repetitive batch experiment enzyme deactivation occurs. It increases by each carried out batch experiment. These facts are substantiated by the corresponding deactivation constants of the first order presented in Table 3.

L-DOPA oxidation catalyzed by L-amino acid oxidases from *Crotalus adamanteus* and *Rhodococcus opacus*

L-amino acid oxidases (L-AAO) from *Crotalus adamanteus* and *Rhodococcus opacus* were applied for biotransformation of 3,4-dihydroxyphenyl-L-alanine (L-DOPA) to 3,4-dihydroxyphenylpyruvic acid (Fig. 7). Kinetic parameters of both enzymes were estimated from the independent experiments by non-linear regression method (Table 4). On the basis of parameter values, these two enzymes were compared[17] in their activity and specificity. The mathematical model was developed (Fig. 8) and validated by the batch reactor experiments (Fig. 9). Additionally, catalytic constant of the enzyme was estimated from the batch reactor experiments using Levenspiel method.

L-amino acid oxidase from *Rhodococcus opacus* was found to have much lower Michaelis-Menten constant, which means that it is more specific to the substrate. It is also substrate inhibited, which is not the case for L-AAO from *Crotalus adamanteus*. By comparing the catalytic constants of these two enzymes it was obvious that the bacterial enzyme is 10-fold more active than the enzyme from *Crotalus adamanteus*. Kinetic parameters also revealed that the bacterial enzyme is far more hydrogen peroxide inhibited in the reactor experiments (experiments without catalase), than the enzyme from the snake venom (Fig. 9A and Table 4). Catalase was necessary in this system to obtain a long-term activity, and to prevent α-keto acid decarboxylation.

Enzyme kinetic modeling was used not only for process prediction but also for comparison of the two investigated enzymes which makes it possible to quantify their differences.

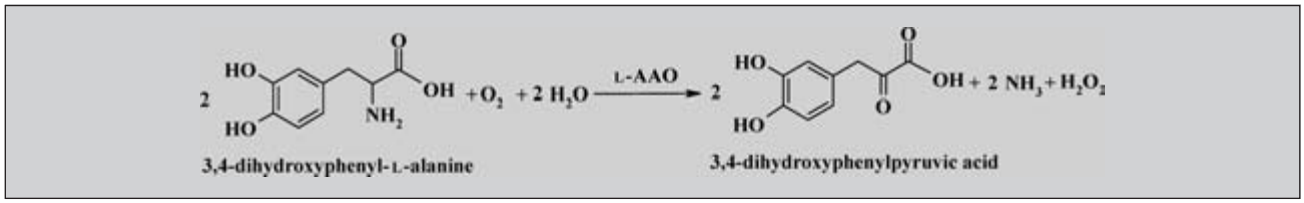

Fig. 7 – *Biotransformation of 3,4-dihydroxyphenyl-L-alanine (L-DOPA) to 3,4-dihydroxyphenylpyruvic acid by L-amino acid oxidases from Crotalus adamanteus and Rhodococcus opacus*

$$r_1 = \frac{V_m \cdot \gamma_{\text{L-AAO}} \cdot c_{\text{L-DOPA}}}{K_m^{\text{L-DOPA}} \cdot \left(1 + \frac{c_{H_2O_2}}{K_i^{H_2O_2}}\right) + c_{\text{L-DOPA}}}$$ L-AAO from *Crotalus adamanteus*

$$r_2 = \frac{V_m \cdot \gamma_{\text{L-AAO}} \cdot c_{\text{L-DOPA}}}{K_m^{\text{L-DOPA}} \cdot \left(1 + \frac{c_{H_2O_2}}{K_i^{H_2O_2}}\right) + c_{\text{L-DOPA}} + \frac{c_{\text{L-DOPA}}^2}{K_i^{\text{L-DOPA}}}}$$ L-AAO from *Rhodococcus opacus*

$$\frac{dc_{\text{L-DOPA}}}{dt} = -r_1 \text{ (or } r_2)$$

Fig. 8 – *Mathematical model for 3,4-dihydroxyphenyl-L-alanine oxidation catalyzed by L-amino acid oxidases from Crotalus adamanteus and Rhodococcus opacus*

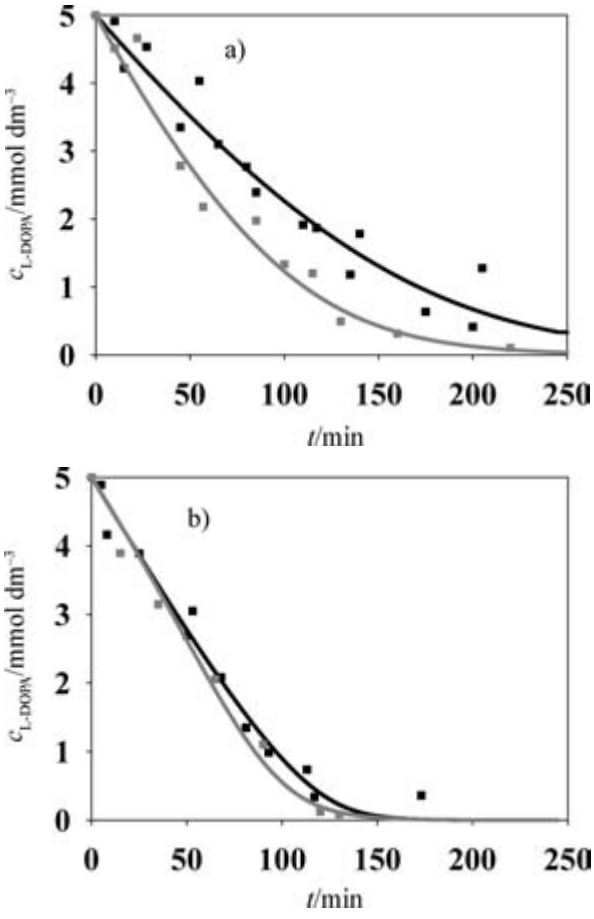

Fig. 9 – *3,4-dihydroxyphenyl-L-alanine oxidation in the batch experiment a) without catalase and b) with catalase.* ■ *L-DOPA concentration in the experiment catalyzed by L-AAO from C.adamanteus,* ■ *L-DOPA concentration in the experiment catalyzed by L-AAO from R. opacus, line — model simulations*

Table 4 – *Kinetic parameters for L-DOPA oxidation catalyzed by L-amino acid oxidase from Crotalus adamanteus and Rhodococcus opacus*

Parameter	*C. adamanteus*		*R. opacus*	
V_m, U mg^{-1}	0.12		0.38	
$K_m^{\text{L-DOPA}}$, mmol dm^{-3}	0.53		0.02	
$K_i^{\text{L-DOPA}}$, mmol dm^{-3}	–		6.69	
	With catalase	Without catalase	With catalase	Without catalase
V_m, U mg^{-1}	0.17	0.12	0.41	0.28
$K_m^{\text{L-DOPA}}$, mmol dm^{-3}	0.60	0.60	0.02	0.01
$K_i^{H_2O_2}$, mmol dm^{-3}	–	2.69	0.11	0.01
$K_i^{\text{L-DOPA}}$, mmol dm^{-3}	–	–	22.06	6.94
k, min^{-1}	0.164	0.114	1.534	1.585

Mathematical models of microbial biotransformation processes

Production of alcohol dehydrogenase (ADH) in baker's yeast growing cells

In the yeast cell, enzyme alcohol dehydrogenase (ADH) is responsible for the synthesis and the oxidation of the ethanol. Ethanol production in yeast occurs when the pyruvate oxidation through the Krebs cycle is stopped due to oxygen insufficiency which is the main driving force for the reac-

tions of this cycle, or if too much pyruvate is being produced from glucose to be oxidised in the mitochondrion[18] (Fig. 10). Regarding the previous fact, the assumption was that the highest ADH production would be achieved during the oxidative-reductive baker's yeast growth. The oxidative growth is necessary for the biomass production because the ADH is intracellular product and the reductive for the ethanol synthesis.[19]

A mathematical model was formulated to simulate cell growth and enzyme production during the aerobic and micro-aerobic growth of the yeast *S. cerevisiae*. Model was based on three metabolic events in the yeast: glucose fermentation, glucose oxidation and ethanol oxidation.[20] Cell growth was expressed as a sum of particular growth rate in different metabolisms (Fig. 11). Their participation to the total specific growth rate depended on the availability of the dissolved oxygen. Michaelis-Menten kinetics was used to describe substrate uptake rate. Enzyme production was assumed as a cell growth associated[21] and enzyme deactivation was described by the first order kinetics.[22]

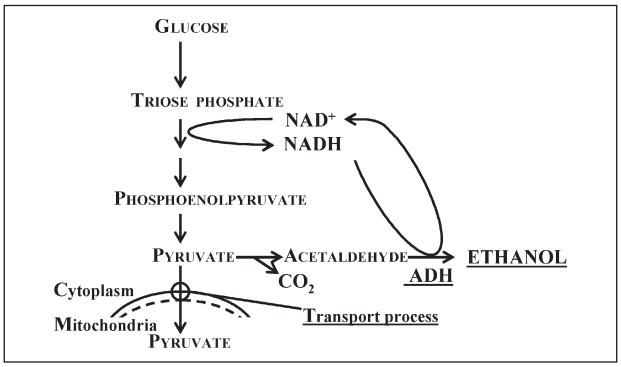

Fig. 10 – *Glucose metabolism at anaerobic conditions*

Parameters were estimated by using the least square method to minimize difference between experimental and calculated values of state variables (confidence was set at 95 %). For this purpose the results of the baker's yeast cultivations at initial glucose mass concentration of 30 g dm^{-3} and at micro-aerobic conditions were used (DO = 10 %). The list of evaluated parameters is given in the Table 5. The results of comparison model and experiment are presented in Fig. 12.[23]

As the enzyme production was shown to be growth associated; with higher biomass concentration higher enzyme activity was expected. Considering, that a higher final biomass concentration could be expected at higher initial glucose concentration or by increasing oxygen supply, model has been validated using higher initial glucose concentration and at aerobic conditions. A good agreement

Glucose uptake rate:

$$r_G = r_{G,max} \cdot \frac{\gamma_G}{K_G + \gamma_G}$$

Glucose uptake rate – oxidative pathway:

$$r_{G,lim} = r_{G,max} \cdot \frac{\gamma_O}{K_O + \gamma_O}$$

$$r_{G,OX} = \min \begin{bmatrix} r_G \\ r_{O,lim} / Y_{O/G} \end{bmatrix}$$

Glucose uptake rate – reductive pathway:

$$r_{G,red} = r_G - r_{G,OX}$$

Ethanol production:

$$r_{Et,pr} = Y_{Et/G} \cdot r_{G,RED}$$

Ethanol uptake rate:

$$r_{Et,up} = r_{Et,max} \cdot \frac{\gamma_{Et}}{K_{Et} + \gamma_{Et}}$$

$$r_{Et,OX} = \min \begin{bmatrix} r_{Et,up} \\ (r_{O,lim} - r_{G,OX} \cdot Y_{OG}) / Y_{O/Et} \end{bmatrix}$$

Oxygen consumption:

$$r_O = Y_{O/G} \cdot r_{G,OX} + Y_{O/Et} \cdot r_{Et,OX}$$

Specific biomass growth rates:

$$\mu_{OX} = Y_{X/G}^{OX} \cdot r_{G,OX}$$

$$\mu_{RED} = Y_{X/G}^{RED} \cdot r_{G,RED}$$

$$\mu_{Et} = Y_{X/Et} \cdot r_{Et/OX}$$

Balance equations:

$$\frac{d\gamma_X}{dt} = (\mu_{OX} + \mu_{RED} + \mu_{Et}) \cdot \gamma_X$$

$$\frac{d\gamma_{Et}}{dt} = (r_{Et,pr} - r_{Et,OX}) \cdot \gamma_X$$

$$\frac{d\gamma_G}{dt} = -(r_{G,OX} - r_{G,RED}) \cdot \gamma_X$$

$$\frac{d\gamma_O}{dt} = k_L a \cdot (\gamma_{O\,SAT} - \gamma_O) - r_O \cdot \gamma_X$$

$$\frac{dA_V}{dt} = a \cdot (\mu_{OX} + \mu_{RED} + \mu_{Et}) \cdot \gamma_X - b\gamma_X$$

Fig. 11 – *Kinetic and mass balance equations for the baker's yeast growth and ADH production in the batch reactor*

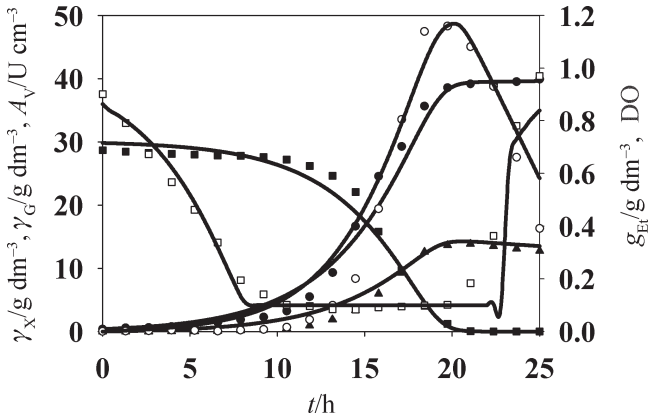

Fig. 12 – *Baker's yeast growth experiment used for the parameter estimation ($\gamma_{G0} \approx 30$ g dm^{-3}, micro-aerobic conditions –DO = 10 %). ●, biomass; ■, glucose; ○, ethanol; ▲, volume ADH activity; □, dissolved oxygen; — model.*

of the result of the experiment and simulation was achieved at micro-aerobic conditions (DO = 10 %) with higher initial glucose mass concentration ($\gamma_{G0} \approx 50$ g dm^{-3}, Fig. 13). At aerobic conditions ($\gamma_{G0} \approx 50$ g dm^{-3}, DO = 40 %), a lower ethanol mass concentration, but a higher biomass concentration was obtained in comparison to the same initial glucose concentration using lower oxygen supply rate (Fig. 13). The parameters a that describes the enzyme activity was not valid for the cultivations under aerobic conditions. Although in both cases the oxidative-reductive metabolism was accomplished, a lower level of ethanol productivity under aerobic conditions caused a lower enzyme production (Fig. 13). For this reason the value of parameter a for the

Table 5 – *Values of parameters for the baker's yeast growth and ADH production*

Parameter	Values
$r_{G,max}$, h^{-1}	0.212
$r_{O,max}$, h^{-1}	0.038
$r_{Et,max}$, h^{-1}	0.072
K_G, g dm^{-3}	0.612
K_O, g dm^{-3}	$9.6 \cdot 10^{-5}$
K_{Et}, g dm^{-3}	0.101
$Y_{X/Et}$, g_{WW} g^{-1}	0.293
$Y_{O/Et}$, g g^{-1}	2.838
$Y_{Et/G}$, g g^{-1}	0.049
$Y_{O/G}$, g g^{-1}	0.515
$Y^{OX}_{X/G}$, g_{WW} g^{-1}	1.521
$Y^{RED}_{X/G}$, g_{WW} g^{-1}	1.051
a, U g_{WW}^{-1}	0.400
b, h^{-1}	0.015

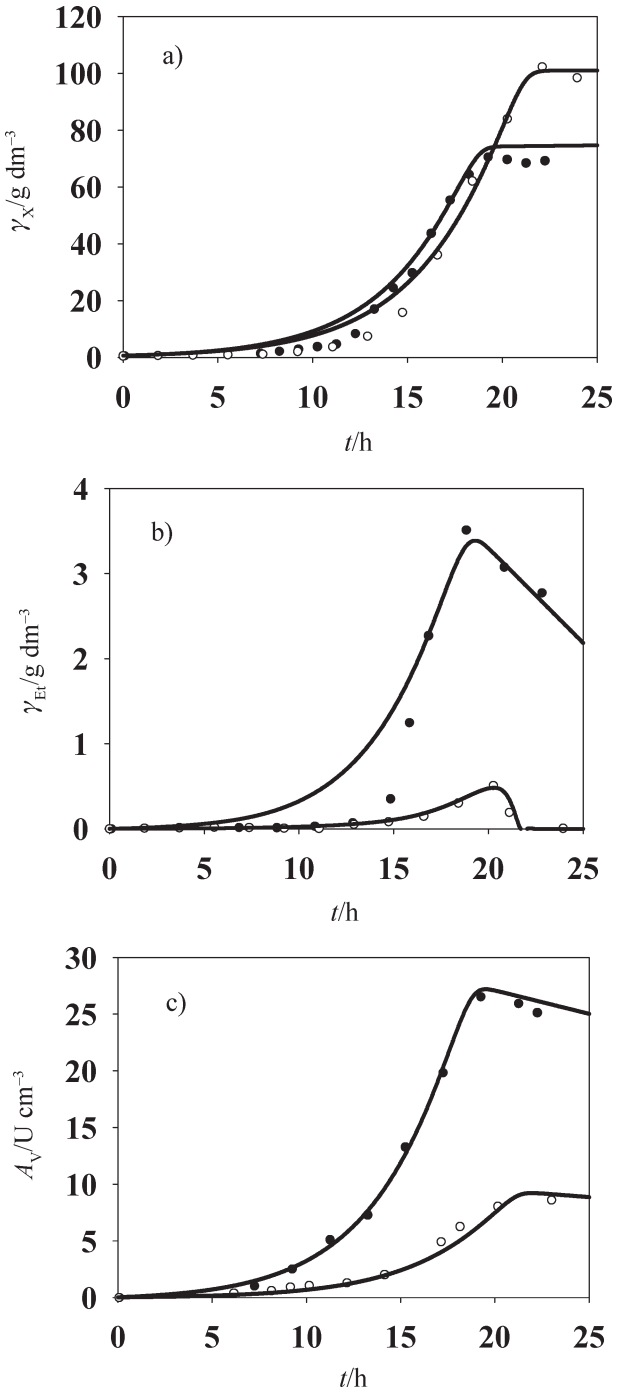

Fig. 13 – *Model validation: biomass wet mass (a), ethanol (b), volume activity changes (c) with time, $\gamma_{G0} \approx 50$ g dm^{-3}. ●, micro-aerobic conditions ($\varphi_{DO} = 10$ %); ○, aerobic conditions (DO = 40 %); – model*

aerobic baker's yeast cultivations is about four fold lower ($a = 0.099 \pm 0.0121$ U g^{-1}) than the one under micro-aerobic conditions (Table 5).

Production of L-malic acid by permeabilized non-growing yeast cells

L-malic acid is produced by the action of enzyme fumarase from fumaric acid.[24] Enzyme fumarase as a biocatalyst can be used in a whole cell[25] or

as a purified enzyme.[26] In the yeast enzyme fumarase is a part of citrate cycle responsible for the biotransformation of fumaric to L-malic acid (Fig. 14). Using the whole cells, the time consuming and expensive operations of enzyme purification are avoided. It preserves the enzyme in its natural environment thus protecting it from inactivation during subsequent use in continuous system.[27] The major limitations which need to be addressed while using such cells are the diffusion of substrate and products through the cell wall, and unwanted side reactions due to the presence of other enzymes. These problems could be obviated by the use of permeabilized cells as a source of enzyme. Permeabilization of the cells removes the barrier for the free diffusion of the substrate/product across the cell membrane, and also empties the cell of most of the small molar mass cofactors, etc., thus minimizing the unwanted side reactions.[28] This fact is very important for the L-malic production by whole cells, because both side reactions in which malic and fumaric acid are involved in the Krebs cycle producing oxalic either succinic acid, require the coenzymes (Fig. 14).

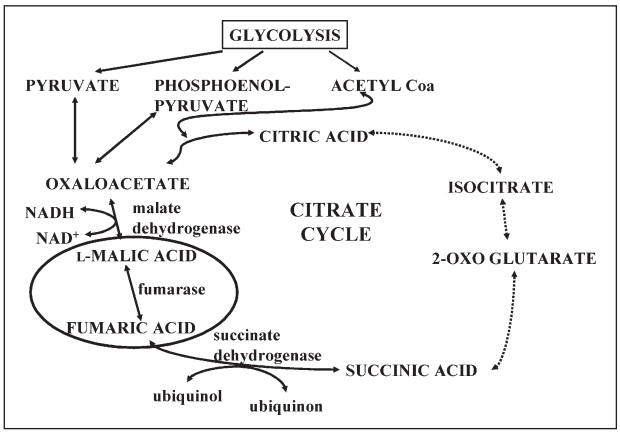

Fig. 14 – *Biotransformation of fumaric to L-malic acid in yeast*

The yeast *Saccharomyces bayanus* (UVAFERM BC), permeabilized for 5 min with $w = 0.2$ % CTAB (Cetyl Trimethyl Ammonium Bromide) as a surfactant (based on the optimization results for the permeabilization procedure[6]) was used as a biocatalyst for the L-malic production. The kinetic activity of fumarase in permeabilized yeast cells was measured by the initial reaction rate method with different concentration of fumaric and malic acid as a substrate. It was found that malic acid inhibits a hydrolysis of fumaric acid. The fumarase kinetics was described using a Michaelis-Menten kinetics with competitive product inhibition. Parameters were estimated by non-linear regression analysis using simplex and least squares method implemented in SCIENTIST software (Table 6).[29]

Table 6 – *Kinetic parameters of fumarase in permeabilized Saccharomyces bayanus cells*

Parameter	Values
V_{m1}, U g_{ww}^{-1}	264.995
K_{m1}, mmol dm^{-3}	18.812
V_{m2}, U g_{ww}^{-1}	84.075
K_{m2}, mmol dm^{-3}	19.360
K_i, mmol dm^{-3}	33.078

The enzyme in permeabilized yeast cells shows about three times higher maximal activity to fumaric acid as a substrate compared to L-malic acid. A relatively high inhibition constant indicates that the enzyme is not strongly inhibited by L-malic acid. The mathematical model for the batch system including the estimated parameters is shown in Fig. 15.[29]

To validate the proposed model L-malic acid production in the batch mode was carried out (Fig. 16). For that purpose several experiments were carried out with permeabilized cells at 3.5 g dm^{-3} and different initial fumarate mass concentration. In all experiments the conversion of cca 80 % was achieved, no side product was detected and C-balance was 100 %. The same conversion can be accomplished using the isolated and purified enzyme fumarase from porcine heart.[26]

Production of 2,5-diketo-D-gluconic acid using *Pantoea citrea*

In recent years a certain amount of attention has been focused on the biosynthesis of the vitamin C precursors. The interest in the diketo-acid fermentation was renewed after the possibility of production of 2-keto-L-gulonic acid (2-KLG), the intermediate in the vitamin C biosynthesis, by a tan-

$$\text{fumaric acid} + H_2O \underset{r_2}{\overset{r_1}{\underset{\text{fumarase}}{\underset{\textit{Sacc. bayamus}}{\rightleftharpoons}}}} \text{L-malic acid}$$

Kinetic equations:

$$r_1 = \frac{V_{m1} \cdot \gamma_{\text{yeast}} \cdot c_{\text{fumaric acid}}}{K_{m1}\,(1 + c_{\text{malic acid}} / K_i) + c_{\text{fumaric acid}}}$$

$$r_2 = \frac{V_{m2} \cdot \gamma_{\text{yeast}} \cdot c_{\text{malic acid}}}{K_{m2} + c_{\text{malic acid}}}$$

Balance equations:

$$\frac{\mathrm{d}c_{\text{fumaric acid}}}{\mathrm{d}t} = r_2 - r_1 \qquad \frac{\mathrm{d}c_{\text{malic acid}}}{\mathrm{d}t} = r_1 - r_2$$

Fig. 15 – *Kinetic and mass balance equations for the L-malic production in the batch reactor by permeabilized Saccharomyces bayanus cells*

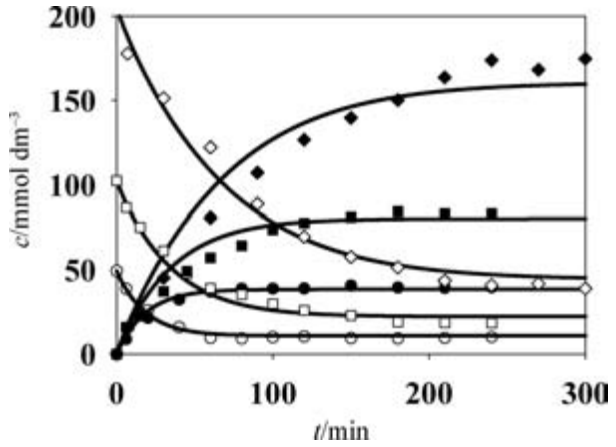

Fig. 16 – *L-malic acid production in the batch reactor by permeabilized Saccharomyces bayanus cells ($c_{fumaric\ acid\ 0}$ = ●○ 50 mmol dm^{-3}, ■□ 100 mmol dm^{-3}, ◆◇ 210 mmol dm^{-3}; white symbols – fumaric acid, black symbols – L-malic acid, — model)*

dem or a co-fermentation.[30] In such a fermentation process glucose is proposed to be oxidized to 2,5-diketo-D-gluconic acid (2,5-DKG) as the first step followed by its stereospecific reduction to 2-KLG. The mixed fermentation with two steps including the application of genetic engineering suggests that the development of promising new processes is able to compete with the classical Reichstein production process.[31]

Bioconversion of glucose to 2,5-diketo-D-gluconic acid was performed in the continuous culture of *Pantoea citrea*. *Pantoea citrea* is a ketogenic organism known to accumulate 2,5-DKG. The dehydrogenation reactions are catalyzed by so called direct membrane-bound NAD(P) independent dehydrogenases i.e. the glucose dehydrogenase (GDH), the gluconic acid dehydrogenase (GADH) and the 2-ketogluconic acid dehydrogenase (2-KGADH) as shown on the Fig. 17.[32] This reaction scheme is based on a common knowledge of the potential metabolic pathways combined with a careful examination of the experimental data.

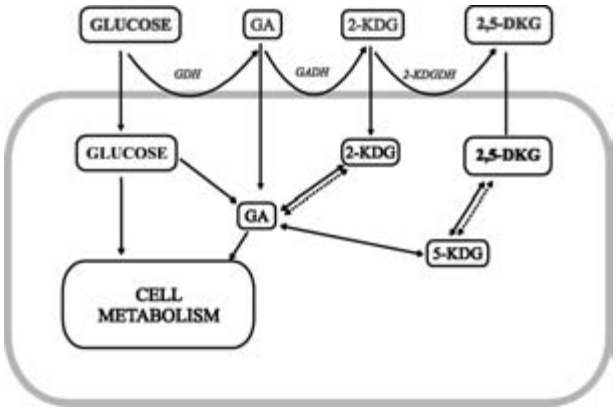

Fig. 17 – *Bioconversion of glucose to 2,5-DKG by Pantoea citrea*

The mathematical model of glucose to 2,5-DKG bioconversion process concerns the change of biomass, substrate and product concentration. It is determined that the biomass grows as well on glucose, gluconic acid, 2-KDG and 2,5-DKG. The r_G, r_{GA} and $r_{2\text{-}KDG}$ express the rates of the reactions catalyzed by GDH, GADH and 2-KGADH. It is assumed that the oxidation kinetics for these reactions can be described by the Michaelis-Menten rate expression referring to each substrate, where the specific rate of consumption is limited by the concentration. The specific growth rate of the biomass was assumed to be the sum of specific growth rate on each substrate. The mathematical model is proposed in accordance with these hypotheses (Fig. 18).

The model parameters were estimated earlier by experiments with the oxygen partial pressure method[33] and on the basis of dynamic responses method.[34] The developed model is compared with experimental data from batch and continuous culture experiment with *Pantoea citrea* for the series of initial glucose concentrations in the medium. A reasonable agreement was observed between the model simulations and the experimental data for the both, batch and continuous culture growth on glucose (Fig. 19A) as well as for the bioprocess products (gluconic acid, 2-keto-D-gluconic acid and 2,5-diketo-D-gluconic acid) (Fig. 19B).

Escherichia coli based pyruvate production

Pyruvic acid and its salts are important chemicals used in the pharmaceutical, food, agrochemical and cosmetic industry. Pyruvate represents one of the most important metabolites in central metabolism of living cells because of its role in the glucose uptake (via carbohydrate phosphoenolpyruvate:phosphotransferase system (pts)), its impact as a precursor for amino acid synthesis, its relevance as an intermediate of glycolysis etc., thus making the metabolite to one of the mostly used reactant in the *Escherichia coli* metabolic network.[35]

Unstructured mathematical model of the pyruvate production process considering the acetate auxotrophic strain *E. coli* YYC202 *ldhA::Kan* was developed. The strain is completely blocked in its ability to convert pyruvate into acetyl-CoA or acetate (using glucose as the carbon source) resulting in an acetate auxotrophy during growth in glucose minimal medium. Because of primary uncertainties regarding the microbial kinetics (and the underlying mechanism) several models for microbial growth and product formation were formulated as a "competing" set of model candidates. For simplification of the model the bioconversion of glucose to pyruvate is regarded as a one-step-enzymatic reaction:

$$C_6H_{12}O_6 \xrightarrow{\textit{Escherichia coli},\ \text{acetate},\ O_2} 2C_3H_4O_3 + 2H_2O$$

Growth kinetics:

$$\mu = \mu_{\mathrm{G}} + \mu_{\mathrm{GA}} + \mu_{\text{2-KDG}} + \mu_{\text{2,5-DKG}}$$

$$\mu_{\mathrm{G}} = \mu_{\mathrm{MAX}}^{\mathrm{G}} \cdot \frac{c_{\mathrm{G}}}{K_{\mathrm{S}}^{\mathrm{G}} + c_{\mathrm{G}}} - m \cdot Y_{\mathrm{X/G}}$$

$$\mu_{\text{2-KDG}} = \mu_{\mathrm{MAX}}^{\text{2-KDG}} \cdot \frac{c_{\text{2-KDG}}}{K_{\mathrm{S}}^{\text{2-KDG}} + c_{\text{2-KDG}}}$$

$$\mu_{\mathrm{GA}} = \mu_{\mathrm{MAX}}^{\mathrm{GA}} \cdot \frac{c_{\mathrm{GA}}}{K_{\mathrm{S}}^{\mathrm{GA}} + c_{\mathrm{GA}}}$$

$$\mu_{\text{2,5-DKG}} = \mu_{\mathrm{MAX}}^{\text{2,5-DKG}} \cdot \frac{c_{\text{2,5-DKG}}}{K_{\mathrm{S}}^{\text{2,5-DKG}} + c_{\text{2,5-DKG}}}$$

Substrate utilization rate:

$$r_i = V_{\mathrm{MAX},i} \frac{c_i}{K_{\mathrm{s},i} + c_i}$$

The unsteady-state material balance for biomass in continuous stirred tank reactor (CSTR)

$$\frac{\mathrm{d}\gamma_{\mathrm{X}}}{\mathrm{d}t} = \mu \cdot \gamma_{\mathrm{X}} - D \cdot \gamma_{\mathrm{X}}$$

The unsteady-state substrate mass balance in CSTR

$$\frac{\mathrm{d}c_{\mathrm{G}}}{\mathrm{d}t} = (c_{\mathrm{G0}} - c_{\mathrm{G}}) \cdot D - \left(m + \frac{1}{Y_{\mathrm{X/G}}} \cdot \mu_{\mathrm{G}} \right) \cdot \gamma_{\mathrm{X}} - r_{\mathrm{G}} \cdot \gamma_{\mathrm{X}}$$

$$\frac{\mathrm{d}c_{\text{2-KDG}}}{\mathrm{d}t} = (c_{\text{2-KDG0}} - c_{\text{2-KDG}}) \cdot D - \frac{1}{Y_{\text{X/2-KDG}}} \cdot \mu_{\text{2-KDG}} \cdot \gamma_{\mathrm{X}} + (r_{\mathrm{GA}} \cdot Y_{\text{2-KDG/GA}} - r_{\text{2-KDG}}) \cdot \gamma_{\mathrm{X}}$$

$$\frac{\mathrm{d}c_{\text{2,5-DKG}}}{\mathrm{d}t} = (c_{\text{2,5-DKG0}} - c_{\text{2,5-DKG}}) \cdot D - \frac{1}{Y_{\text{X/2,5-DKG}}} \cdot \mu_{\text{2,5-DKG}} \cdot \gamma_{\mathrm{X}} + r_{\text{2-KDG}} \cdot Y_{\text{2,5-DKG/2-KDG}} \cdot \gamma_{\mathrm{X}}$$

F i g . 1 8 – *Kinetics and mass balance equations for 2,5-diketo-D-gluconic acid production by Pantoea citrea in the continuous culture*

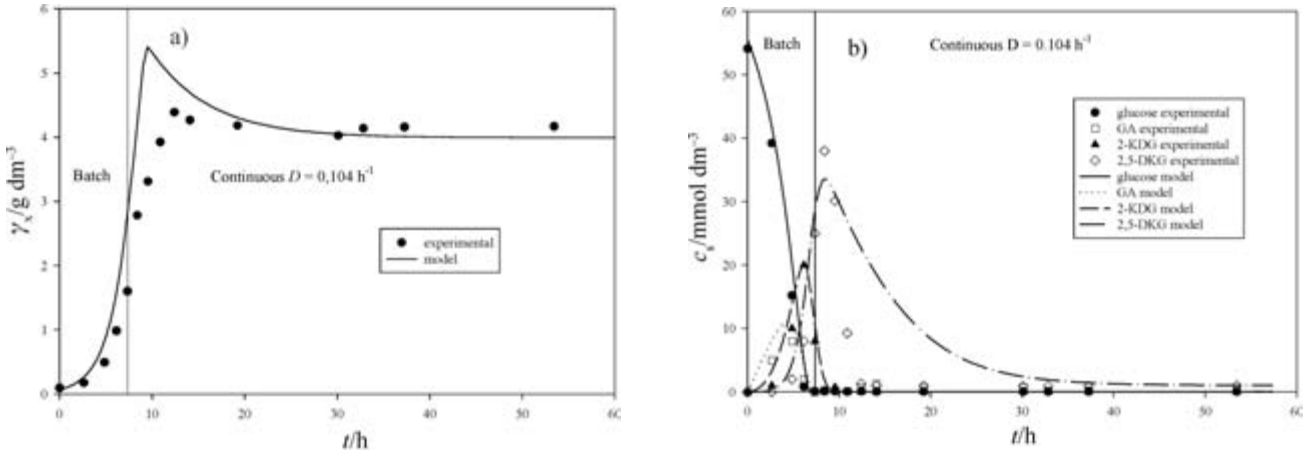

F i g . 1 9 – *Experimental data and model simulation results of the batch and continuous culture experiments for a) biomass growth, and b) biotransformation of glucose to 2,5-DKG*

Following constrains were used to define all of the models: glucose and acetate are only limiting substrates; cell growth occurs only in the presence of both substrates; there was no oxygen effect on biomass growth and pyruvate production; product formation kinetics should combine growth associated and non-growth associated characteristics; bioconversion of glucose to pyruvate was assumed

to be a one step enzymatic reaction; both biomass growth and pyruvate production were inhibited by high pyruvate concentrations; the viscosity of the reaction mixture remains constant during experiments and potential mixing effects of the highly concentrated feed with the cultivation medium are neglected in order to protect model simplicity. To model the microbial specific growth rate various, well-known approaches were tested e.g. multiple substrates Monod kinetics, Levenspiel model, the model of Jerusalimsky, Monod kinetics with substrate inhibition, and Andrews kinetics. Additionally, different kinds of product formation kinetics were evaluated for example modified Michaelis-Menten equation for non-competitive product inhibition, Luedeking-Piret equation, and modified Luedeking-Piret equation with the Levenspiel term.[36]

Parameter estimation was carried out using data from fed-batch fermentation performed at constant glucose feed rates. While the model identification was realized by least-square method, the model discrimination was based on the Model Selection Criterion (MSC).[39] The validation of model parameters was performed applying data from two different fed-batch experiments. Consequently, the most suitable model was identified that reflected the pyruvate and biomass curves adequately by considering a pyruvate inhibited growth (Jerusalimsky approach) and pyruvate inhibited product formation (described by modified Luedeking-Piret/Levenspiel term) (Fig. 20).

Using this modeling approach, an acceptable model prediction for cell growth and pyruvate formation was achieved (Fig. 21), which are both essential variables to model process alternatives and scale-ups. The predicted biomass and pyruvate concentrations of developed model are in a good agreement with the experimental data. On the basis of a single criterion, the residual sum of squares, devel-

Growth kinetics:

$$\mu = \mu_{MAX} \cdot \frac{\gamma_G}{K_S^G + \gamma_G} \cdot \frac{\gamma_A}{K_S^A + \gamma_A} \cdot \frac{K_P}{(\gamma_P + K_P)}$$

Substrate uptake:

$$r_G = \frac{\mu}{Y_{X/G}}$$

$$r_A = \frac{\mu}{Y_{X/A}}$$

$$Y_{X/G} = \frac{Y_{X/G,MAX} \cdot \mu}{Y_{X/G,MAX} \cdot m_G + \mu}$$

$$Y_{X/A} = \frac{Y_{X/A,MAX} \cdot \mu}{Y_{X/A,MAX} \cdot m_A + \mu}$$

Product formation rate:

$$r_P = \left(\alpha \cdot \frac{d\gamma_X}{dt} + \beta \cdot \gamma_X\right) \cdot \left(1 - \frac{\gamma_P}{\gamma_{P,MAX}}\right)$$

Mass balances for the fed-batch process:

$$\frac{d\gamma_X}{dt} = -\frac{q_V}{V} \cdot \gamma_X + \mu \cdot \gamma_X$$

$$\frac{d\gamma_G}{dt} = -\frac{q_V}{V} \cdot \gamma_G + \frac{q_{VG}}{V}\gamma_{G,0} - r_G \cdot \gamma_X - r_P \cdot \gamma_X$$

$$\frac{d\gamma_A}{dt} = -\frac{q_V}{V} \cdot \gamma_A + \frac{q_{VA}}{V}\gamma_{A,0} - r_A \cdot \gamma_X$$

$$\frac{d\gamma_P}{dt} = -\frac{q_V}{V} \cdot \gamma_P + r_P \cdot \gamma_X \cdot Y_{P/G}$$

$$\frac{dV}{dt} = q_{VG} + q_{VA} = q_V$$

F i g . 2 0 – *Kinetics and mass balance equations for the fed-batch pyruvate production process using Escherichia coli*

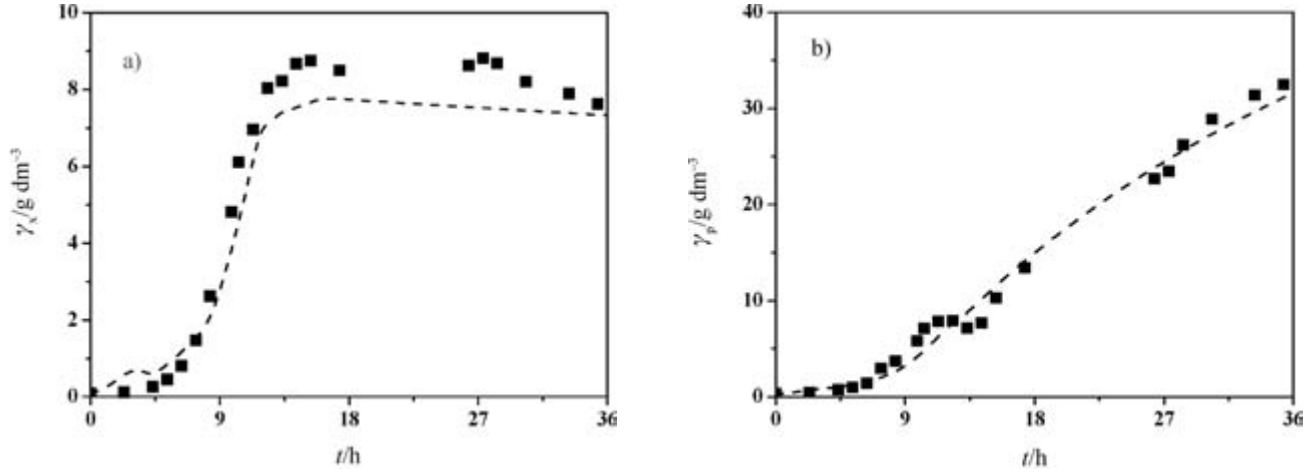

F i g . 2 1 – *Data obtained by models simulation and experimental data for a) biomass (■) and b) pyruvate (●) concentration in fed-batch process*

oped model was favored because it achieved the lowest residual sum of squares. Additionally, the estimated parameters in this model have acceptable confidence interval and the model is mechanistically correct. Furthermore, selected model is mechanistically the most accurate one because it contains all experimentally observed effects: growth inhibition by pyruvate and pyruvate inhibited product (pyruvate) formation.

Numerical methods

The parameters of all described models are estimated by non-linear least squares regression and are optimized using the Nelder-Mead algorithm.[37] The numerical values of the parameters were evaluated by fitting the model to the experimental data with the "Scientist" software.[38] The model differential equations were solved numerically by the fourth order Runge-Kutta algorithm, which is also offered in the same software.

The calculated data are compared with the experimental data, recalculated in the optimization routine and fed again to the integration step until minimal error between experimental and integrated values was achieved (built-in Scientist). The residual sum of squares is defined as the sum of the squares of the differences between experimental and calculated data. For discrimination of various models, the minimal value of the residual sum of squares and the MSC criterion[39] have been used as trial functions. The MSC attempts to represent the "information content" of a given set of parameter estimates by relating the coefficient of determination to the number of parameters (or equivalently, the number of degrees of freedom) that were required to obtain the fit. When comparing two models with different numbers of parameters, this criterion imposes a burden on the model with more parameters. The most appropriate model will be the one with the largest MSC.

The "Episode" algorithm for stiff system of differential equations, implemented in the "Scientist" software package, was used for the simulations. It uses variable coefficient Adams-Moulton and Backward Differentiation Formula methods in the Nordsieck form, treating the Jacobian matrix as full or banded.

Conclusion

Modeling and simulation have a large potential in searching for optimal process conditions, development and process design, control, and scale-up of the biotransformation processes. In combination with modern computer techniques modeling and evaluation of the results can be used to identify the cost structure of the process, to document and quantify process improvements, and to compare process alternatives. Additionally, modeling and simulation leads to better understanding and quantification of the investigated process and could lead to significant material and costs savings especially in the early phases of the process development. Modeling and simulation enable maximal advantage in use of available process data. In this work it was shown that simple, easy to use, and robust models are suitable to describe both, enzymatic and microbial biotransformation processes, and to support different engineering tasks.

Abbreviations

2-KDG – 2-keto-D-gluconic acid
2-KGADH – 2-ketogluconic acid dehydrogenase
2-KLG – 2-keto-L-gulonic acid
2,5-DKG – 2,5-diketo-D-gluconic acid
A – acetate
ADH – alcohol dehydrogenase
CSTR – continuous stirred tank reactor
D-AAO – D-amino acid oxidase
D-met – D-methionine
DO – dissolved oxygen
Et – ethanol
EMR – enzyme membrane reactor
G – glucose
GA – gluconic acid
GADH – gluconic acid dehydrogenase
GDH – glucose dehydrogenase
L-AAO – L-amino acid oxidase
L-DOPA – 3,4-dihydroxyphenyl-L-alanine
MSC – Model Selection Criterion
O – oxygen
OX – oxidative growth mechanism
P – pyruvate
RED – reductive growth mechanism
X – biomass

List of symbols

A – activity, U cm^{-3}
a – activity of enzyme, U g^{-1}
b – deactivation coefficient, h^{-1}
c – concentration, mmol dm^{-3}
D – dilution rate, min^{-1}
K_m – Michaelis-Menten constant, mmol dm^{-3}
k – catalytic constant of the enzyme, min^{-1}
k_d – enzyme deactivation constant, min^{-1}
$k_L a$ – transfer coefficient, min^{-1}

m – coefficient, min^{-1}
q_V – volume flow rate, $dm^3\ min^{-1}$
r – reaction rate, U cm^{-3}
T – temperature, °C
t – time, min, h
V – volume, dm^3
V_m – maximal reaction rate, U cm^{-3}, U mg^{-1}, U g^{-1}
Y – yield
μ – specific growth rate, min^{-1}
τ – residence time, min^{-1}
γ – mass concentration, g dm^{-3}

References

1. *Vasić-Rački, Đ.,* History of industrial biotransformations–Dreams and Realities, in *Liese, A., Seelbach, K., Wandrey, C.* (Ed.), Industrial Biotransformations, Wiley-VCH, Weinheim, 2006, pp 1-36.
2. *Biwer, A. P., Zuber, P. T., Zelić, B., Gerharz, T., Bellmann, K. J., Heinzle, E.,* Ind. Eng. Chem. Res. **44** (2005) 3124.
3. *van Can, H. J. L., te Braake, H. A. B., Hellinga, C., Luyben, K. C. A. M., Heijnen, J. J.,* Biotechnol. Bioeng. **54** (1997) 549.
4. *Versyck, K. J., Claes, J. E., Van Impe, J. F.,* Math. Comput. Simulat. **46** (1998) 621.
5. *Lednicky, P., Meszaros, A.,* Bioprocess Eng. **18** (1998) 427.
6. *Pertev, C., Türker, M., Berber, R.,* Comput. Chem. Eng. **21** (1997) S739.
7. *Horiuchi, J.-I.,* J. Biosci. Bioeng. **94** (2002) 574.
8. *Adour, L., Amrane, A., Progent, Y.,* J. Chem. Technol. Biotechnol. **77** (2002) 1300.
9. *Srivastava, A. K., Giridhar, R.,* J. Chem. Technol. Biotechnol. **73** (1998) 23.
10. *Vasić-Rački, Đ., Kragl, U., Liese, A.,* Chem. Biochem. Eng. Q. **7** (2003) 7.
11. *Vasić-Rački, Đ., Bongs, J., Schörken, U., Sprenger, G. A., Liese, A.,* Bioprocess. Biosyst. Eng. **25** (2003) 285.
12. *Kula, M. R., Wichmann, R., Oden, U., Wandrey, C.,* Biochimie **62** (1980) 523.
13. *Caron, D., Coughlan, A. P., Simard, M., Bernier, J.,* Biotechnol. Lett. **27** (2005) 713.
14. *Findrik, Z., Vasić-Rački, Đ., Lütz, S., Daußmann, T., Wandrey, C.*, Biotechnol. Lett. **27** (2005) 1087.
15. *Wichmann, R., Vasić-Rački, Đ.*, Advances in Biochemical Engineering/Biotechnology **92** (2005) 225.
16. *Findrik, Z., Vasić-Rački, Đ., Geueke, B., Kuzu, M., Hummel, W.*, Eng. Life Sci. **5** (2005) 550.
17. *Findrik, Z., Geueke, B., Hummel, W., Vasić-Rački, Đ.,* Biochem. Eng. J. **27** (2006) 275.
18. *Ratledge, C.*, Bioprocess Eng. **6** (1991) 195.
19. *Fowler, M. W.*, Enzyme Technology**,** Biotechnology for Engineers, Wiley & Sons, 1988, pp 180-185.
20. *Sonnleitner, B., Käppeli, O.*, Biotechnol. Bioeng. **28** (1986) 927.
21. *Luedeking, R., Piret, E. L.,* Biotechnol. Bioeng. **67** (2000) 633.
22. *Miron, J., Gonzalez, M. P., Pastrana, L., Murado, M. A.,* Enzyme Microb. Tech. **31** (2002) 615.
23. *Vrsalović Presečki, A., Vasić-Rački, Đ.,* Proc. Biochem. **40** (2005) 2781.
24. *Marconi, W., Faiola, F., Piozzi, A.*, J. Mol. Catal. B-Enzym. **15** (2001) 93.
25. *Chibata, I., Tosa, T., Takata, I.* **1** (1983) 9.
26. *Giorno, L., Drioli, E., Carvoli, G., Cassano, A., Donato, L.*, Biotechnol. Bioeng. **72** (2001) 77.
27. *D'Souza, S. F.*, Biosens. Bioelectron. **16** (2001) 337.
28. *D'Souza, S. F.*, Curr. Sci. India **77** (1999) 69.
29. *Vrsalović Presečki, A.*, *Vasić-Rački, Đ.*, Biotechnol. Lett. **27** (2005) 1835.
30. *Sonoyama, T., Tani, H., Matenda, K., Kageyama, B., Tanimoto, M., Kobayashi, K., Kyotani, H., Mitsushima, K.,* Appl. Environ. Microbiol. **43** (1982) 1064.
31. *Boudrant, J.,* Enzyme Microb. Technol. **12** (1990) 322.
32. *Qazi, G. N., Sharma, N., Parshad, R.,* J. Ferm. Bioeng. **76** (1993) 336.
33. *Zelić, B., Pavlović, N., Delić, V., Vasić-Rački, Đ.*, Bioprocess Eng. **21** (1999) 45.
34. *Zelić, B., Pavlović, N., Vasić-Rački, Đ.* in: Specific processes and technologies, Proceedings of 2nd European Congress of Chemical Engineering, Montpellier, France, **71** (1999) 303
35. *Zelić, B., Gostovic, S., Vuorilehto, K., Vasić-Rački, Đ., Takors, R.,* Biotechnol. Bioeng. **85** (2004) 638.
36. *Zelić, B., Vasić-Rački, Đ., Wandrey, C., Takors, R.,* Bioprocess Biosyst. Eng. **26** (2004) 249.
37. *Nelder, J. A., Mead, R.,* Comput. J. **7** (1965) 308.
38. SCIENTIST handbook, MicroMath®, Salt Lake City, 1986-1995.
39. *Akaike, H.,* Math. Sci. **14** (1976) 5.